Plasma channel formed by ultraviolet laser pulses at 193 nm in air

Yuanyuan Ma (马媛媛)[1,2], Xin Lu (鲁 欣)[1], Tingting Xi (奚婷婷)[2,4], Qihuang Gong (龚旗煌)[1], and Jie Zhang (张 杰)[1,2,3*]

[1]*State Key Laboratory for Mesoscopic Physics, Department of Physics, Peking University, Beijing 100871, China*

[2]*Laboratory of Optical Physics, Institute of Physics, Chinese Academy of Sciences, Beijing 100190, China*

[3]*Department of Physics, Shanghai Jiao Tong University, Shanghai 200240, China*

[4]*Department of Physics, Graduate University of Chinese Academy of Sciences, Beijing 100049, China*

[*]*E-mail: jzhang@aphy.iphy.ac.cn*

Received May 12, 2009

The propagation of picosecond deep ultraviolet laser pulse at wavelength of 193 nm in air is numerically investigated. Long plasma channel can be formed due to the competition between Kerr self-focusing and ionization induced defocusing. The plasma channel with electron density of above $10^{13}/\mathrm{cm}^3$ can be formed over 70 m by 50-ps, 20-mJ laser pulses. The fluctuation of laser intensity and electron density inside ultraviolet (UV) plasma channel is significantly lower than that of infrared pulse. The linear absorption of UV laser by air is considered in the simulation and it is shown that the linear absorption is important for the limit of the length of plasma channel.

OCIS codes: 320.5550, 320.7110, 320.7090.

doi: 10.3788/COL20090709.0865.

In recent years, the ultrashort laser pulse filamentation has attracted a great interest[1−10]. Filamentation is the result of a dynamic balance between nonlinear Kerr self-focusing and plasma defocusing, which is induced by high-order multiphoton ionization (MPI) of air. Long distance plasma channel with good spatial continuity is necessary for some applications such as lighting control and guiding of long gap air discharge.

Much of the theoretical and experimental work on filamentation was concentrated on the infrared (IR) laser pulse, typically at the wavelength of 800 nm and pulse durations around dozens or hundreds of femtoseconds[4]. In the well known case of 800-nm wavelength, the Kerr effect is proportional to the laser intensity I, but the ionization rate of oxygen molecular is proportional to I^8. The balance between the Kerr self-focusing and ionization defocusing is highly dynamic for 800-nm laser pulse. If the laser pulse is initially focused by a convex lens, the length of the formed filament is only several meters long with the electron density of $10^{16}-10^{17}/\mathrm{cm}^3$ [1]. If the laser pulses freely propagate in air without initial focusing, the length of filament can extend to hundreds of meters but the electron density is very low for experiment detection. As a result, the study of producing long range plasma channel with good spatial continuity is still a big challenge in this field.

It has been proposed that ultraviolet (UV) filaments with long pulse duration would produce long plasma channel[10]. Schwarz *et al.*[11] performed experiments using a hybrid Ti:sapphire/KrF excimer laser to obtain filaments at 248 nm. The pulse duration was between 600 fs and several picoseconds. They observed filaments with the propagation distance of 12 m. Tzortzakis *et al.*[12,13] performed experiments using 248-nm laser pulse for both 450 and 5 ps. The created filament can survive for 4 m.

There are also several deep UV short laser pulses that can be produced by a hybrid excimer laser system, such as ArF at 193 nm and F_2 at 157 nm. Zhu *et al.* achieved 10-mJ picosecond radiation tunable from 195 to 210 nm by sum-frequency mixing of the fundamental and the third harmonic of Ti:sapphire laser pulses[14]. This situation gives us possibilities to scale forward to the filamentation on shorter wavelength. If the laser wavelength is shorter than 200 nm, the energy of two photons is enough to ionize the oxygen molecular. In this case, the ionization rate is proportional to I^2. Therefore, the focusing and defocusing effect should be easier to get balanced, in comparison with longer wavelength. This behavior of deep UV laser pulse is beneficial to form plasma channel with good continuity and more uniform distribution of electron density. Motivated by the advantages of deep UV laser pulses mentioned above, we numerically study the nonlinear propagation of picosecond 193-nm UV laser pulses in air. The critical power P_{cr} for self-focusing effect is about 30 MW. It is found that a long and continuous plasma channel can be formed by the 50-ps laser pulse with the initial power $10P_{\mathrm{cr}}$. The length of the produced plasma channel is about 75 m with the intensity above 10^9 W/cm^2 and the electron density around $1.3\times10^{13}-1.3\times10^{14}$ /cm^3. The effect of linear absorption of UV laser in air is also considered.

The nonlinear propagation of deep UV laser pulse can by described by extended nonlinear Schrödinger (NLS) equation for slowly varying envelope of a linearly polarized laser electric field. The NLS equation is written

as[15]

$$\frac{\partial E}{\partial z} = \frac{\mathrm{i}}{2k_0}\Delta_\perp E - \mathrm{i}\frac{k''}{2}\frac{\partial^2 E}{\partial t^2} + \mathrm{i}k_0 n_2 |E|^2 E - \mathrm{i}k_0\frac{n_\mathrm{e}}{2n_\mathrm{c}}E - \frac{\sigma}{2}n_\mathrm{e}E - \frac{\alpha}{2}n_O E - \frac{\beta^{(K)}}{2}|E|^{2K-2}E. \quad (1)$$

The equation is expressed in the reference frame moving with the pulse group velocity ($t \to t - z/v_g$). The central wave number $k_0 = 2\pi/\lambda_0$, where $\lambda_0 = 193$ nm is the central wavelength of the laser pulse. The terms on the right-hand side of Eq. (1) account for the transverse diffraction with $\Delta_\perp \equiv \frac{\partial^2}{\partial r^2} + \frac{1}{r}\frac{\partial}{\partial r}$ in cylindrical symmetry, the group velocity dispersion with coefficient $k'' = \partial^2 k/\partial\omega^2|\omega_0$, Kerr self-focusing, the plasma defocusing induced by multiphoton ionization (MPI) with electron density n_e, the power dissipation caused by plasma absorption, linear absorption, and multiphoton absorption (MPA). The cross section for inverse Bremsstrahlung following the Drude model $\sigma = k_0\omega_0\tau_c/\left[n_0 n_\mathrm{air}\left(1+\omega_0^2\tau_c^2\right)\right]$, where τ_c denotes the characteristic time for electron-neutral inverse bremsstrahlung. $n_\mathrm{O} = 0.2n_\mathrm{air} = 5\times10^{18}/\mathrm{cm}^3$ denotes the density of oxygen molecules. The linear absorption of UV laser by air should not be ignored due to the large cross-section $\alpha = 1.613\times10^{-23}$ cm^2 [16]. We ignore the effect of self-steepening and space-time focusing. These effects mainly influence the temporal characteristics of the pulses which are not the main interest of our work[17]. We also ignore the delayed Kerr effect because no spectral redshifting has been measured for UV beams[4] and the pulse duration we used is much more than the relaxation time of air.

The generation of plasma by multiphoton and avalanche ionization is described by the evolution equation for the electron density:

$$\frac{\partial n_\mathrm{e}}{\partial t} = \frac{\beta^{(K)}}{K\hbar\omega_0}|E|^{2K}\left(1 - \frac{n_\mathrm{e}}{n_\mathrm{air}}\right) + \frac{\sigma}{U_i}n_\mathrm{e}|E|^2. \quad (2)$$

For MPI of oxygen molecules with the ionization potential $U_i = 12.1$ eV, $K = \mathrm{mod}\left(U_i/\hbar\omega_0 + 1\right)$ is the minimum number of photons required to liberate an electron. The coefficient $\beta^{(K)} = \hbar\omega K\rho_\mathrm{at}\sigma_K$ can be computed from Keldysh's theory. Electron recombination which becomes efficient on long time scales (ns) is ignored[18,19]. All coefficients in Eqs. (1) and (2) are summarized in Table 1.

The initial envelop of laser pulse with input power P_in can be written as

$$E(r,t,0) = \sqrt{2P_\mathrm{in}/\pi r_0^2}\,\mathrm{e}^{-r^2/r_0^2 - t^2/t_\mathrm{p}^2}. \quad (3)$$

The critical power P_cr for self-focusing effect is about 30 MW. In self-guided propagation mode, the intensity is saturated by plasma defocusing[23]. This enables us to roughly link the peak intensity to the maximum electron density on the propagation axis $r = 0$ as[19]

$$n_2 I \sim \frac{n_\mathrm{e}(I)}{2n_\mathrm{c}}, \quad (4)$$

Table 1. Coefficients in Eqs. (1) and (2)

Symbol	Value	Units	Notes
λ_0	193	nm	Wavelength
k''	1.586	fs^2/cm	Group velocity dispersion[20]
n_2	2.01×10^{-18}	cm^2/W	Nonlinear index[17]
K_O	2	-	Multiphoton ionization order[21,22]
$\beta^{(K)}$	5.275×10^{13}	cm^{2k-3}/W^{k-1}	Multiphoton ionization rate[21,22]
σ	3.08×10^{-21}	cm^2	Cross-section for inverse Bremsstrahlung[21,22]
α	1.613×10^{-23}	cm^2	Cross-section for linear absorption

where $n_\mathrm{c} = \varepsilon_0 m\omega^2/e^2$ is the critical plasma density, with m being the mass of electron, ω the laser angular frequency, and e the elementary charge. When avalanche ionization is negligible, $n_\mathrm{e}(I)$ can be estimated by direct integration of Eq. (2):

$$n_\mathrm{e}(I) \sim \sigma^{(K)} I^K n_\mathrm{air} t_\mathrm{p}. \quad (5)$$

From Eqs. (4) and (5), the clamping intensity is given by

$$I_\mathrm{clamp} \sim \left(\frac{2n_\mathrm{c}n_2}{\sigma^{(K)}n_\mathrm{air}t_\mathrm{p}}\right)^{1/(K-1)}. \quad (6)$$

This yields the clamping intensity I_clamp $\sim1.8\times10^9$ W/cm^2 for laser pulse with pulse duration $t_\mathrm{p} = 50$ ps.

In the simulation, Eq. (1) is solved using full-step (not split-step) fast Fourier transformation in time and Crank-Nicholson in transverse space dimension. The whole time interval is discretized into 1024 points and the resolution is 248 fs. In the radial direction, we adopt a nonuniform grid division. The number of spatial grid is 400 with the spatial resolution 8.9 μm in the filament region and 60 μm in the fringe. The spatial resolution is enough to describe the micron size filaments and basically indicate the characteristics of thin filaments. The grid size of the propagation distance is 1 mm, which is defined to guarantee convergence of the algorithm.

Firstly, we consider the propagation of a 50-ps Gaussian pulse with 3-mm transverse waist. For the numerical results presented below, we alter the initial laser power in order to generate a single plasma channel with perfect properties. Figure 1 shows the energy fluence distribution defined as $F(r,z) = \int_{-\infty}^{+\infty}|E(r,t,z)|^2\mathrm{d}t$ for laser pulses with different input powers. Figure 2 displays the radius, peak intensity, and peak electron density of

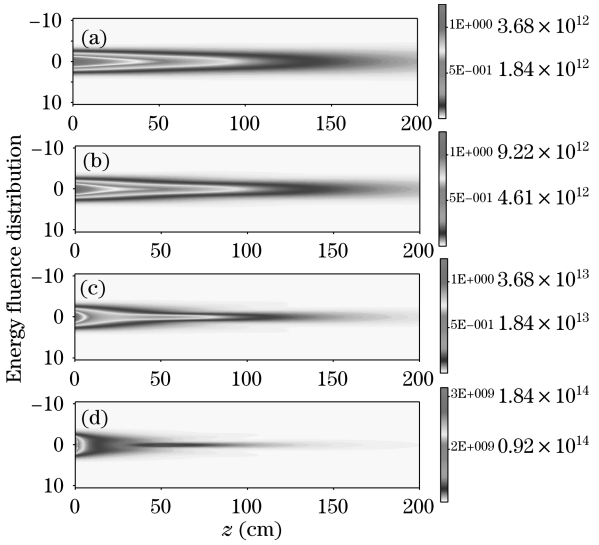

Fig. 1. Energy fluence distribution of laser pulse with different input energies of (a) $P_{\rm in} = P_{\rm cr}$, (b) $P_{\rm in} = 2.5P_{\rm cr}$, (c) $P_{\rm in} = 10P_{\rm cr}$, and (d) $P_{\rm in} = 50P_{\rm cr}$.

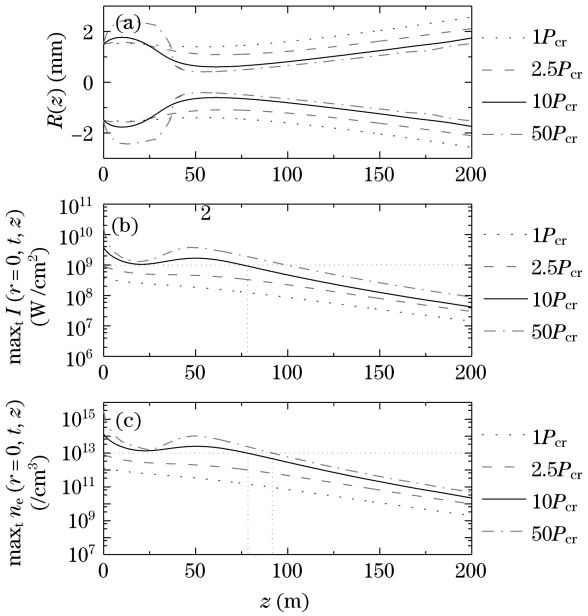

Fig. 2. (a) Beam radius, (b) peak intensity, and (c) electron density as functions of z for the laser pulse with input powers of $P_{\rm cr}$, $2.5P_{\rm cr}$, $10P_{\rm cr}$, and $50P_{\rm cr}$.

the plasma channels predicted by the numerical computations. The radius of the beam, $R(z)$, is taken at the half maximum of the fluence distribution. With one or several critical power ($P_{\rm in} = P_{\rm cr}$ and $P_{\rm in} = 2.5P_{\rm cr}$), the beam radius maintains almost the initial beam size over 100 m. Self-focusing is not observed due to the linear absorption and plasma defocusing as shown in Figs. 1(a), (b), and Fig. 2(a). The energy fluence always decreases along the propagation distance. In Fig. 1(c), the input laser power is $10P_{\rm cr}$ and the initial intensity of laser pulse is around the clamping intensity. The corresponding input laser energy is 10 mJ. The triggered initial electron density is 1.3×10^{14} /cm^3. The ionization rate is proportional to I^2 which is stronger than the Kerr self-focusing effect. Hence, the laser pulse is strongly defocused by the

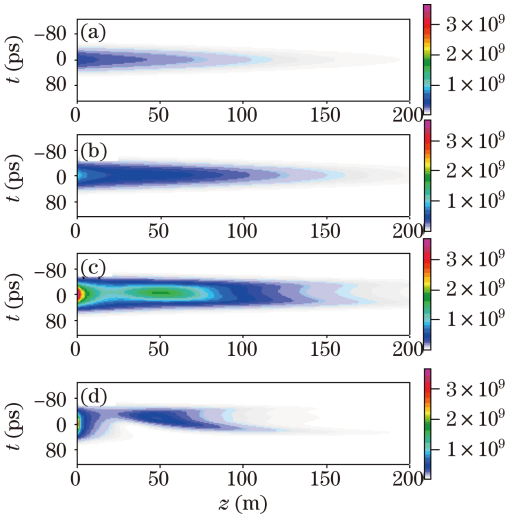

Fig. 3. Temporal evolution of the laser pulse with different input powers of (a) $P_{\rm in} = P_{\rm cr}$, (b) $P_{\rm in} = 2.5P_{\rm cr}$, (c) $P_{\rm in} = 10P_{\rm cr}$, and (d) $P_{\rm in} = 50P_{\rm cr}$.

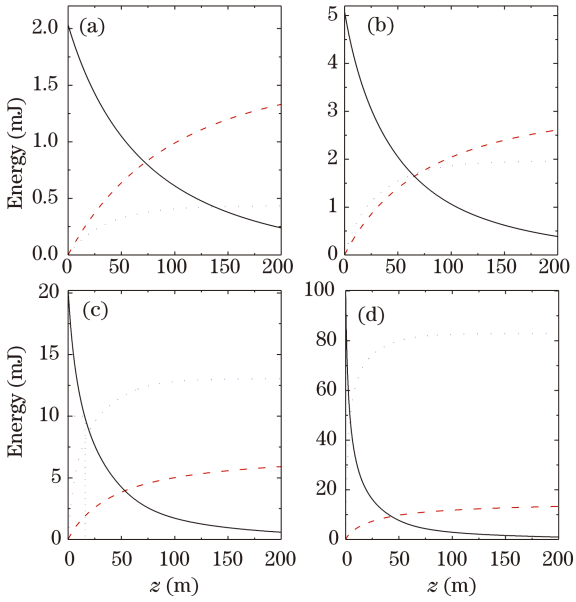

Fig. 4. Energy evolution (solid line), linear absorption (dashed line), and multiphoton absorption (dotted line) of a 3-mm waist, 50-ps laser beam at 193 nm with different input powers of (a) $P_{\rm in} = P_{\rm cr}$, (b) $P_{\rm in} = 2.5P_{\rm cr}$, (c) $P_{\rm in} = 10P_{\rm cr}$, and (d) $P_{\rm in} = 50P_{\rm cr}$.

plasma generated in the early propagation range. Then the laser pulse exhibits one focusing and defocusing cycle as the pulse propagates. The beam radius maintains 1.2−1.5 mm in the propagation range of $40<z<100$ m. The length of plasma channel is defined when the electron density is above 1.0×10^{13} /cm^3 which is sufficient for lightning initiation[24]. The plasma channel survives for 80 m with intensity $I>10^9$ W/cm^2 and plasma density $n_{\rm e}>1.0\times 10^{13}$ /cm^3. After propagating for about 100 m, the energy loss due to MPA and linear absorption of UV laser by air terminates the channeling. When the input power is $50P_{\rm cr}$ (Fig. 1(d)), the triggered initial electron density is 3.3×10^{15} /cm^3 and it decreases to 10^{13} /cm^3 in the first defocusing stage. We can find

that the energy loss is much higher than that in Fig. 1(c) because of the significantly higher MPA during the propagation. Hence, the energy is dispersed outside and the beam radius is broadened, thus allowing the beam to self-focus again. The beam maintains a diameter of 0.8−1.1 mm for $40<z<100$ m. The plasma channel survives for about 90 m with the electron density above 1.0×10^{13} /cm^3 (Fig. 2(c)). Figure 3 shows the temporal evolution of the laser pulses along the propagation axis. It is seen that in the case of $P_{\rm in} = 10P_{\rm cr}$, the pulse maintains a shape almost unaffected along the plasma range (Fig. 3(c)). With higher input power $P_{\rm in} = 50P_{\rm cr}$, the pulse splits and leads to a forklike pattern, where two arms of a fork corresponds to the leading (negative times) and trailing (positive times) split pulses. These results allow us to easily conclude that the input power should not be very high in order to reach a quasi-stable state.

In our simulations, the electron density is 3−7 orders of magnitude lower than the density of oxygen molecules of air. As a result, from Eq. (1) we can estimate that the plasma absorption can be ignored compared with linear absorption of UV laser pulse in air. Figure 4 displays the total energy evolution and energy loss due to linear absorption and MPA of the UV laser pulse with different input powers. With the critical power $P_{\rm cr}$ (Fig. 4(a)), the linear absorption is dominant due to the weak ionization of air. If the input power is 2.5 times higher than $P_{\rm cr}$ (Fig. 4(b)), the energy loss due to ionization is at the same level of linear absorption. With a higher input power (Figs. 4(c), (d)), we can find the energy of the laser pulse decreases much quicker in the first propagation range with higher input energy because of the significantly high MPA. However, linear absorption of UV laser pulse by air dominates in the further propagation and limits the length of the plasma channel.

In conclusion, the propagation of picosecond laser pulses at 193 nm is numerically investigated. Compared to the laser pulse with long wavelength, the defocusing and self-focusing effect are easy to get balance to form a quasi-static plasma channel at the wavelength of 193 nm. In our simulation, a 75-m long plasma channel is formed by 20-mJ, 50-ps laser pulses. The fluctuation of electron density inside plasma channel is lower than that of infrared pulse. The linear absorption of UV laser pulses by air is an important factor to limit the length of plasma channel for long range propagation.

This work was supported by the National Natural Science Foundation of China (Nos. 60621063, 10634020, 10734130, and 10521002) and the National "973" Program of China (Nos. 2007CB815101 and 2006CB806007).

References

1. A. Couairon and A. Mysyrowicz, Physics Reports **441,** 47 (2007).
2. J. Kasparian and J.-P. Wolf, Opt. Express **16,** 466 (2008).
3. L. Bergé and S. Skupin, Phys. Rev. Lett. **100,** 113902 (2008).
4. A. Couairon and L. Bergé, Phys. Rev. Lett. **88,** 135003 (2002).
5. X. M. Zhao, J.-C. Diels, C. Y. Wang, and J. M. Elizondo, IEEE J. Quantum Electron. **31,** 599 (1995).
6. J. Kasparian, R. Ackermann, Y.-B. André, G. Méchain, G. Méjean, B. Prade, P. Rohwetter, E. Salmon, K. Stelmaszczyk, J. Yu, A. Mysyrowicz, R. Sauerbrey, L. Wöste, and J.-P. Wolf, Opt. Express **16,** 5757 (2008).
7. B. La Fontaine, F. Vidal, Z. Jiang, C. Y. Chien, D. Comtois, A. Desparois, T. W. Johnston, J.-C. Kieffer, and H. Pépin, Phys. Plasmas **6,** 1615 (1999).
8. W. Liu, Q. Luo, and S. L. Chin, Chin. Opt. Lett. **1,** 56 (2003).
9. L. Ding, J. Song, Z. Sun, L. Deng, and Z. Wang, Chin. Opt. Lett. **4,** 617 (2006).
10. T. A. Niday, E. M. Wright, M. Kolesik, and J. V. Moloney, Phys. Rev. E **72,** 016618 (2005).
11. J. Schwarz, P. Rambo, J.-C. Diels, M. Kolesik, E. M. Wright, and J. V. Moloney, Opt. Commun. **180,** 383 (2000).
12. S. Tzortzakis, B. Lamouroux, A. Chiron, M. Franco, B. Prade, A. Mysyrowicz, and S. D. Moustaizis, Opt. Lett. **25,** 1270 (2000).
13. S. Tzortzakis, B. Lamouroux, A. Chiron, S. D. Moustaizis, D. Anglos, M. Franco, B. Prade, and A. Mysyrowicz, Opt. Commun. **197,** 131 (2001).
14. J. Zhu, W. Ling, Z. Wang, P. Wang, J. Sun, Z. Wei, D. Zhang, X. Ma, and W. Zhan, Appl. Opt. **46,** 6228 (2007).
15. Y. T. Li, T. T. Xi, Z. Q. Hao, Z. Zhang, X. Y. Peng, K. Li, Z. Jin, Z. Y. Zheng, Q. Z. Yu, X. Lu, and J. Zhang, Opt. Express **15,** 17973 (2007).
16. "AMP:CfA molecular data" http://www.cfa.harvard.edu /amp /ampdata/cfamols.html (March 23, 2009).
17. A. Couairon, S. Tzortzakis, L. Bergé, M. Franco, B. Prade, and A. Mysyrowicz, J. Opt. Soc. Am. B **19,** 1117 (2002).
18. A. Couairon, Appl. Phys. B **76,** 789 (2003).
19. S. Champeaux, L. Bergé, D. Gordon, A. Ting, J. Peñano, and P. Sprangle, Phys. Rev. E **77,** 036406 (2008).
20. G. Wan and Z. Han, Opt. Precision Eng. (in Chinese) **2,** (3) 27 (1994).
21. M. D. Perry, O. L. Landen, A. Szöke, and E. M. Campbell, Phys. Rev. A **37,** 747 (1988).
22. V. Yu. Fedorov and V. P. Kandidov, Opt. Spectrosc. **105,** 280 (2008).
23. J. Kasparian, R. Sauerbrey, and S. L. Chin, Appl. Phys. B **71,** 877 (2000).
24. M. Nicolet, Pure Appl. Geophys. **118,** 3 (1980).